Construction of zwitterionic osmolyte-based hydrogel electrolyte towards stable zinc anode for durable aqueous zinc ion storage and integrated electronic

Tianlong Wu[a], Chenchen Ji[a,b,*], Hongyu Mi[a,*], Fengjiao Guo[a], Gaozhi Guo[a], Biao Zhang[a], Mingzai Wu[c,*]

[a] State Key Laboratory of Chemistry and Utilization of Carbon Based Energy Resources, School of Chemical Engineering and Technology, Xinjiang University, Urumqi 830017, P. R. China. E-mail: jichenchen2010@163.com; mmihongyu@163.com

[b] State Key Laboratory of Fine Chemicals, Dalian University of Technology, Dalian 116024, P. R. China

[c] School of Materials Science and Engineering, Key Laboratory of Structure and Functional Regulation of Hybrid Materials, Ministry of Education, Anhui University, Hefei 230601, P. R. China. Email: wumz@ahu.edu.cn

1. Experimental section

1.1 Synthesis of the hydrogel electrolytes

0.25 g sodium alginate powders were added into 12.5 mL deionized (DI) water at 64 °C for 2 h with a constant stirring rate. After that, 2 g acrylamide monomer was added to the solutions under stirring for 3 h at room temperature. A homogeneous and transparent solution containing 6 mg *N*, *N*′-methylenebisacrylamide and 0.062 g Irgacure 2959 was added to the above-mixed dispersion. Then, the resultant dispersion was transferred into a glass mold followed by triggering under ultra-violet (UV) irradiation via a photopolymerization process (wavelength of 365 nm and intensity of 8 W) for 1 h to form the sodium alginate/polyacrylamide (denoted as SP) hydrogel.[1] After being dehydrated for 5 h under room temperature, the resultant hydrogel was immersed in an SBMA-$Zn(CF_3SO_3)_2$-water ternary-component disperse system (1 M Zn $(CF_3SO_3)_2$ and 40 wt% SBMA aqueous disperse system) at room temperature for 12 h. After that, the sodium alginate/polyacrylamide/ SBMA/$Zn(CF_3SO_3)_2$ zwitterion osmotic hydrogel electrolyte (denoted as SPS-Zn)

was obtained. For comparison, the sodium alginate/polyacrylamide/$Zn(CF_3SO_3)_2$ hydrogel electrolyte (denoted as SP-Zn) was also synthesized by immersing the SP hydrogel into 1 M $Zn(CF_3SO_3)_2$ aqueous solution without SBMA osmolytes.

1.2 Preparation of HCNFs

0.88 g polyvinyl alcohol (PVA) powders were dispersed into 5 mL DI water at 90 °C for 4 h under stirring. After cooling down to room temperature, 5 mL polytetrafluoroethylene (PTFE) water emulsion (60 wt.% of solid content) was then added to the above PVA disperse system and stirred for 24 h. After that, the electrospinning process was conducted under a feed rate of 1.5 mL h^{-1} with a voltage of 16 kV and an 18 cm distance between the drum collector and the needle at room temperature. After the electrospinning process, the as-obtained fibers were kept in a vacuum oven at 65 °C for 12 h. Subsequently, the fibers were calcined at 800 ℃ for 2 h under an argon atmosphere. After cooling down to room temperature, the honeycomb carbon nanofibers (denoted as HCNFs) were obtained.[2, 3]

1.3 Assembly of aqueous and quasi-solid-state ZHSC devices

The cathode mixture paste consists of ethanol, 80 wt% HCNFs active materials, 10 wt% acetylene black, and 10 wt% of PTFE. Then, the obtained slurry was rolled into a round sheet, and further dried at 65 °C for 5 h. Finally, this round sheet was pressed on a flexible graphite paper (the mass loading of active materials is about 2.0 mg cm^{-2}) to obtain the cathode. Aqueous Zn//HCNFs ZHSC was assembled by using the HCNFs cathode, Zn foil (thickness: 80 μm) anode, a Whatman GF/D (Glass Microfiber Filters) separator, and 1 M aqueous $Zn(CF_3SO_3)_2$ electrolyte. The aqueous Zn//HCNFs ZHSC was encapsulated in the CR2032 coin-type battery shell. The quasi-solid-state device was assembled by HCNFs cathode, Zn foil anode, and SA/PAAm/SBMA/$Zn(CF_3SO_3)_2$ hydrogel electrolyte. The quasi-solid-state device was further packaged with polyimide tape to prevent a decrease in the water content of the hydrogel.

1.4 Material characterizations

Field emission scanning electron microscopy (FESEM, SU-8010) was used to reveal the microstructures of the prepared hydrogel samples. The Fourier transform infrared

spectroscopy (VERTEX 70) measurement was used to reveal the chemical components. Nitrogen adsorption/desorption isotherms and pore size distributions were obtained by the 3H-2000PM1/2 equipment at 77 K. The tensile and compressive tests were carried out by attaching the hydrogels to two clips using a tensile machine (ZQ-990LB). The tensile tests were performed on hydrogel samples with a specimen size of 20.0×10.0×1.5 mm^3 at 150 mm min^{-1}. The compression tests were carried out on a cylinder (12 mm in diameter and 25 mm in height). The adhesion strength was revealed by the lap-shear measurement via the universal test machine (ZQ-990LB). A piece of the hydrogel with a specimen size of 20×25×1.5 mm^3 was sandwiched between two substrates (e.g., carbon paper, copper sheet, and zinc sheet) that were fixed to a glass slide using double-faced adhesive tape. The strain sensing tests were performed using a multimeter (DMM6500, 4523760, Keithley).

1.5 Electrochemical measurements

The electrochemical measurements were performed on an electrochemical workstation (CHI760E, Chenhua Instruments, China) and a battery test system (M340A). The linear polarization curves were obtained in a three-electrode system, which involves two Zn foils (as the working and the counter electrodes, respectively) and a saturated calomel reference electrode (SCE)) at 0.1 mV s^{-1}. The cycling performance of the Zn//Zn symmetric cells and Zn//Cu asymmetric cells with an electrode area of 1.1304 cm^2 was measured on an M340A Land battery test system. The CV measurement was carried out on a CHI760E electrochemical analyzer. The galvanostatic charge/discharge (GCD) tests, the self-discharge curves, and cycling stability tests were conducted on an M340A Land battery test system. The specific capacity (C, mAh g^{-1}) and energy density (E, Wh kg^{-1}) were obtained from the M340A Land battery test system. The power density (P, W kg^{-1}) was calculated as follows:[4]

$$P = \frac{3600E}{t} \tag{1}$$

where E (Wh kg^{-1}) represents the energy density, and t (s) is the discharging time.

1.6 Density functional theory (DFT) calculations

The binding energy calculations were done using the Gaussian 16 program.[5] Density functional theory (DFT)[6] calculations with the B3LYP-D3 functional[7, 8] and the 6-311G+(2d, 2p) basis set[9] were used to locate all the stationary points involved. The binding energy (E_b) is defined as follows:

$$E_b = E_{A+B} - (E_A + E_B) \quad (2)$$

Where E_{A+B} is the total energy of the combined A and B, $E_A + E_B$ is the sum of the total energies of A and B before the combination. A and B refer to Zn^{2+} and $CF_3SO_3^-$ or SBMA species, respectively.

DFT calculations for the adsorption energy were performed by using the Vienna Ab-initio Simulation Package (VASP).[10, 11] The exchange-correlation interactions were described by generalized gradient approximation (GGA)[12] with the Perdew–Burke–Ernzerhof (PBE) functional.[13] Spin-polarization was included in all the calculations and a damped van der Waals correction was incorporated using Grimme's scheme to better describe the non-bonding interactions.[14] The cut-off energies for plane waves were set to be 500 eV, and the residual force and energy on each atom during structure relaxation converged to 0.005 eV $Å^{-1}$ and 10^{-5} eV, respectively. The adsorption energy (E_{ad}) is defined as follows:

$$E_{ad} = E_{Zn002+ads} - E_{ads} - E_{Zn002} \quad (3)$$

Where $E_{Zn002+ads}$ is the total energy of Zn (002) crystal plane adsorbed with H_2O/SBMA, E_{ads} is the total energy of SBMA/H_2O, E_{Zn002} is the total energy of Zn (002) crystal plane.

The geometries of SBMA molecule, water molecule, and clusters of mSBMA-$[Zn(H_2O)_n]^{2+}$ (n + m = 6, n = 2 ~ 6) were optimized under the framework of DFT with PBE0 functional[15] and def2SVP basis set.[16] To describe the solvation effect, the SMD (Solvation Model Based on Density)[17] implicit solvent model was used in the following calculations. The DFT-D3 dispersion correction method was also applied in these calculations. The solvation Gibbs free energy of mSBMA-$[Zn(H_2O)_n]^{2+}$ clusters were calculated from the formula:

$$\Delta G = G(\text{mSBMA-}[Zn(H_2O)_n]^{2+}, \text{aq}) - G(\text{Zn, gas}) - n \times G(H_2O, \text{aq}) - m \times G(\text{SBMA, aq}) \quad (4)$$

The electrostatic surface potential (ESP) was calculated using Multiwfn program[18, 19] and then rendered using GaussView Program.

2. Results and discussion

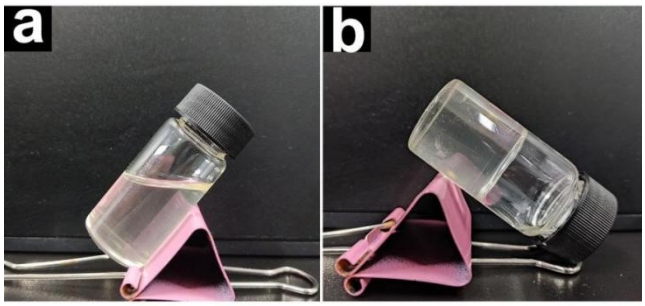

Fig. S1 The preparation of the dual cross-linked SP hydrogels via a UV irradiation process.

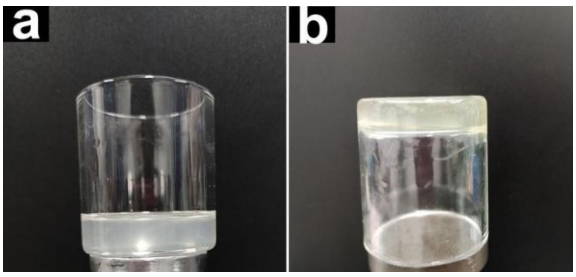

Fig. S2 The optical photographs of (a) the initial 40% SBMA-Zn$(CF_3SO_3)_2$-water ternary-component disperse system, and (b) the residual disperse system gradually evolved into a hydrogel after immersing the SP hydrogel for 12 hours.

Fig. S2 shows that the SBMA-Zn$(CF_3SO_3)_2$-water ternary-component disperse system gradually evolved into a hydrogel after immersing the SP hydrogel for 12 h.

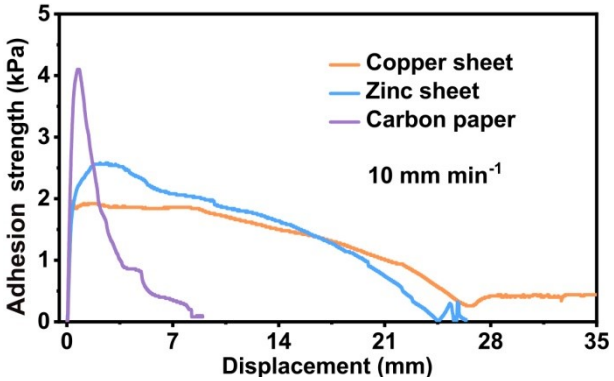

Fig. S3 The lap shear curves of the SPS-Zn hydrogel on different substracts.

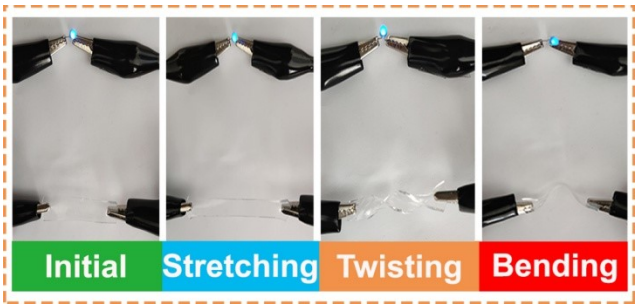

Fig. S4 Photos of the conductive SPS-Zn hydrogel as the circuit at stretching, twisting, and bending states.

Fig. S4 demonstrates that the stretchable SPS-Zn exhibits stable electrical conductivity upon deformation.

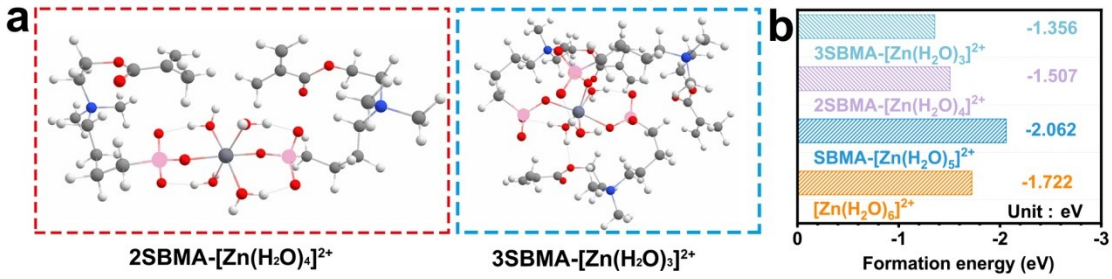

Fig. S5 (a) The hydration structures of the 2SBMA-$[Zn(H_2O)_4]^{2+}$ and 3SBMA-$[Zn(H_2O)_3]^{2+}$. (b) The formation energy for each model.

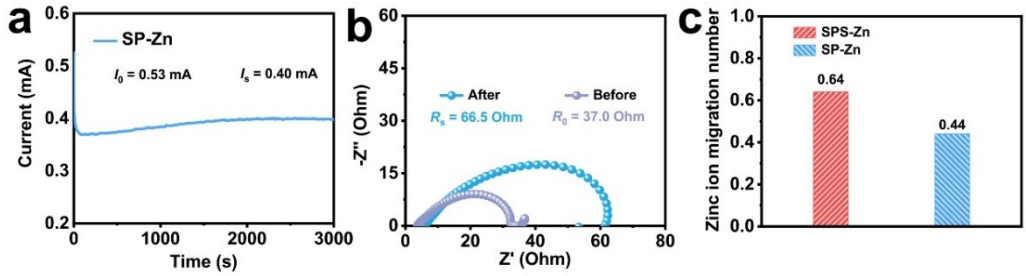

Fig. S6 (a) The *I-t* curve of the Zn|SP-Zn|Zn cell. (b) Nyquist plots of the symmetric cells with Zn electrodes and SP-Zn hydrogel before and after polarization at an applied voltage of 10 mV. (c) Zn^{2+} transference numbers of SPS-Zn and SP-Zn hydrogel electrolytes.

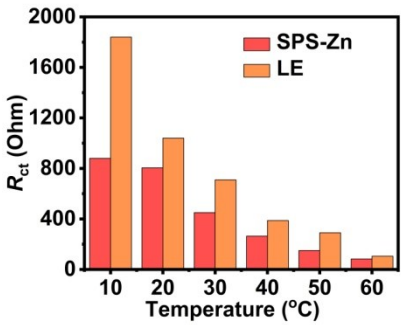

Fig. S7 The R_{ct} values of the Zn|SPS-Zn|Zn and Zn|LE|Zn cells at various temperatures.

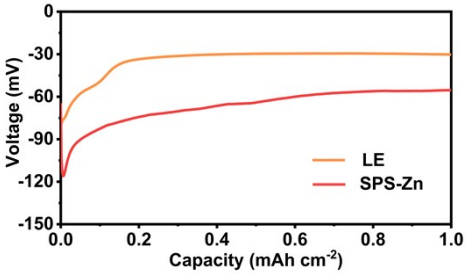

Fig. S8 NOP of Zn ions on Zn foil in different electrolytes.

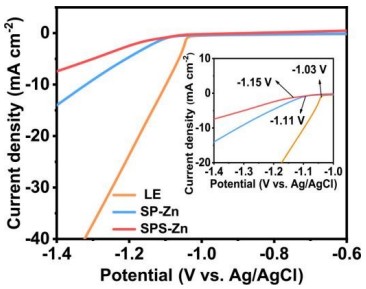

Fig. S9 Linear sweep voltammograms (LSV) curves measured in LE, SP-Zn, and SPS-Zn under a three-electrode system at 1 mV s^{-1}.

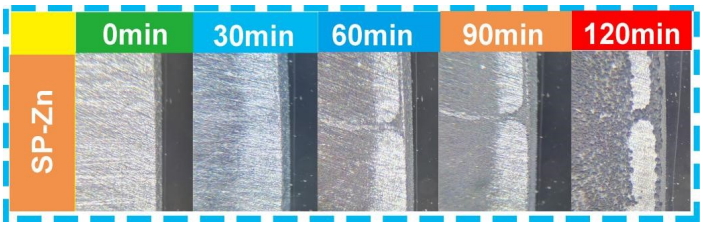

Fig. S10 *In-situ* optical microscopic images for the Zn deposition process in SP-Zn.

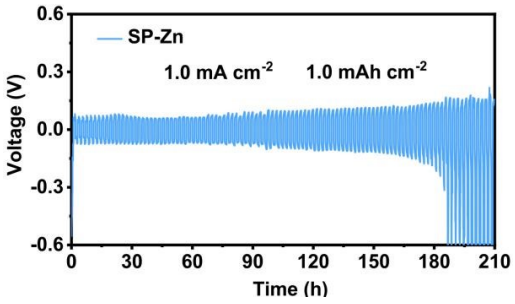

Fig. S11 Cycling tests of the Zn||Zn symmetric cell in SP-Zn at 1 mA cm^{-2} and 1 mAh cm^{-2}.

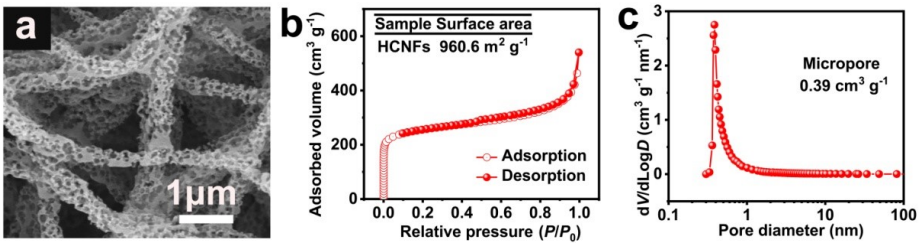

Fig. S12 (a) SEM image, (b) N_2 adsorption/desorption isotherms, and (c) pore size distribution of HCNFs.

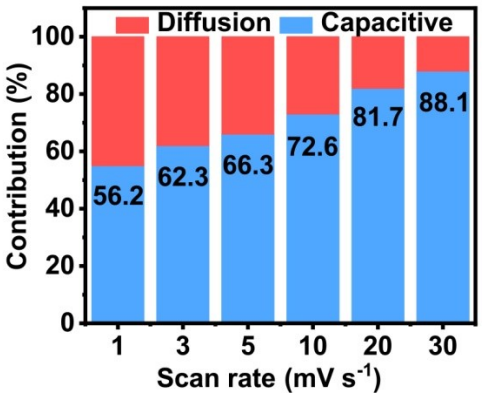

Fig. S13 The capacitive and diffusion contributions at various scan rates of the quasi-solid-state Zn||SPS-Zn||HCNFs ZHSC.

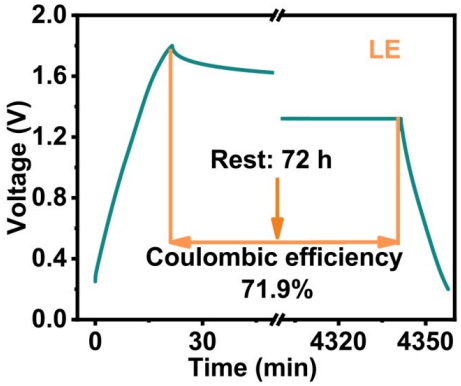

Fig. S14 The self-discharge curve of the ZHSC in LE.

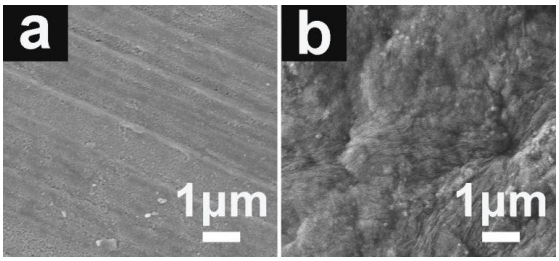

Fig. S15 SEM images of the Zn anodes (a) before and (b) after cycling.

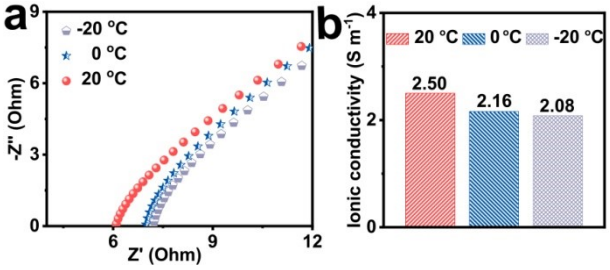

Fig. S16 EIS spectra for the SPS-Zn hydrogel electrolytes tested at various temperatures and the corresponding ionic conductivity data of the SPS-Zn hydrogel electrolyte at various temperatures.

Notes and references

1. X. Sui, H. Guo, P. Chen, Y. Zhu, C. Wen, Y. Gao, J. Yang, X. Zhang and L. Zhang, *Adv. Funct.*

Mater., 2019, **30**, 1907986.
2. K. Dong, J. Liang, Y. Wang, Z. Xu, Q. Liu, Y. Luo, T. Li, L. Li, X. Shi, A. M. Asiri, Q. Li, D. Ma and X. Sun, *Angew. Chem. Int. Ed.,* 2021, **60**, 10583-10587.
3. J. Yan, K. Dong, Y. Zhang, X. Wang, A. A. Aboalhassan, J. Yu and B. Ding, *Nat. Commun.,* 2019, **10**, 5584.
4. C. Ji, D. Wu, Z. Liu, H. Mi, Y. Liao, M. Wu, H. Cui, X. Li, T. Wu and Z. Bai, *ACS Appl. Mater. Interfaces,* 2022, **14**, 23452–23464.
5. M. J. Frisch, G. W. Trucks, H. B. Schlegel, G. E. Scuseria, M. A. Robb, J. R. Cheeseman, G. Scalmani, V. Barone, G. A. Petersson, H. Nakatsuji, X. Li, M. Caricato, A. V. Marenich, J. Bloino, B. G. Janesko, R. Gomperts, B. Mennucci, H. P. Hratchian, J. V. Ortiz, A. F. Izmaylov, J. L. Sonnenberg, Williams, F. Ding, F. Lipparini, F. Egidi, J. Goings, B. Peng, A. Petrone, T. Henderson, D. Ranasinghe, V. G. Zakrzewski, J. Gao, N. Rega, G. Zheng, W. Liang, M. Hada, M. Ehara, K. Toyota, R. Fukuda, J. Hasegawa, M. Ishida, T. Nakajima, Y. Honda, O. Kitao, H. Nakai, T. Vreven, K. Throssell, J. A. Montgomery Jr., J. E. Peralta, F. Ogliaro, M. J. Bearpark, J. J. Heyd, E. N. Brothers, K. N. Kudin, V. N. Staroverov, T. A. Keith, R. Kobayashi, J. Normand, K. Raghavachari, A. P. Rendell, J. C. Burant, S. S. Iyengar, J. Tomasi, M. Cossi, J. M. Millam, M. Klene, C. Adamo, R. Cammi, J. W. Ochterski, R. L. Martin, K. Morokuma, O. Farkas, J. B. Foresman and D. J. Fox, Gaussian 16 Revision. A.03, Gaussian Inc., Wallingford, CT, 2016.
6. Parr, R. G., Yang, W. Density functional theory of atoms and molecules [M]. *Oxford: Oxford University Press*, 1989.
7. A. D. Becke, *J. Chem. Phys.,* 1993, **98**, 5648-5652.
8. C. Lee, W. Yang and R. G. Parr, *Phys. Rev. B,* 1988, **37**, 785-789.
9. K. B. Wiberg, *J. Comput. Chem.,* 1986, **7**, 379-379.
10. G. Kresse and J. Furthmüller, *Comp. Mater. Sci.,* 1996, **6**, 15-50.
11. G. Kresse and J. Furthmüller, *Phys. Rev. B,* 1996, **54**, 11169-11186.
12. J. P. Perdew, K. Burke and M. Ernzerhof, *Phys. Rev. Lett.*, 1996, **77**, 3865-3868.
13. J. P. Perdew, M. Ernzerhof and K. Burke, *J. Chem. Phys.,* 1996, **105**, 9982-9985.
14. S. Grimme, *J. Comput. Chem.,* 2006, **27**, 1787-1799.
15.C. Adamo and V. Barone, *J. Chem. Phys.,* 1999, **110**, 6158-6170.
16.F. Weigend and R. Ahlrichs, *Phys. Chem. Chem. Phys.,* 2005, **7**, 3297-3305.
17. A. V. Marenich, C. J. Cramer and D. G. Truhlar, *J. Phys. Chem. B,* 2009, **113**, 6378-6396.
18.T. Lu and F. Chen, *J. Comput. Chem.,* 2012, **33**, 580-592.
19.T. Lu and F. Chen, *J. Mol. Graph. Model.,* 2012, **38**, 314-323.